Numerical Solution for Three-Dimensional Inviscid Supersonic Flow

P. D. THOMAS,* M. VINOKUR,† R. A. BASTIANON,‡ AND R. J. CONTI*
Lockheed Palo Alto Research Laboratory, Palo Alto, Calif.

An exact finite-difference solution is developed for steady, inviscid, supersonic flow over smooth three-dimensional bodies. The method is applied to a blunt delta wing having straight leading edges and an elliptical cross section. Results are presented for angles of attack up to 30° in both perfect gas and equilibrium air at typical freestream conditions for space shuttle orbiter re-entry. The effects of angle of attack on shock layer structure, on surface pressure distributions, and on surface streamline patterns are investigated. Marked variations are found in the structure of the entropy layer over different portions of the surface; the implications for boundary-layer heat-transfer analyses are discussed.

1. Introduction

PROMINENT among the problems that must be met in the design of lifting re-entry vehicles, such as the space shuttle orbiter, is that of predicting aerodynamic forces and heat transfer in the supersonic flight regime.

The conventional assumption that dissipative effects are confined to a thin viscous boundary layer outside of which the flow is substantially inviscid can be justified throughout a significant portion of this regime. This paper describes a technique for predicting the inviscid flow, and its application to investigate the structure of the flowfield about a blunt delta body.

Problems in the category described are presently tractable only by numerical methods employing digital computers. Although the flow is essentially steady, considerable work has been done in the finite-difference solution of such flows as the time-asymptotic limit of an unsteady flow.[1-3] The advantage of this approach is that the problem is posed as an initial value problem, for which a variety of numerical solution techniques have been developed. However, because the speed and storage capacity of current generation computers are limited, the time-asymptotic method is useful only for small spatial regions, such as the domain of subsonic and transonic flow near the nose of a blunt vehicle. Furthermore, some investigators have encountered difficulties in attempting to extend such solutions into regions of wholly supersonic flow.

On the other hand, in regions of locally supersonic flow, the governing equations are hyperbolic and the steady flow problem itself is well posed as an initial value problem. Elimination of the time dimension then affords a considerable reduction in computer storage requirements and in computation time. Numerical work along these lines has followed two approaches: one based on the method of characteristics, which has a long history of application to two-dimensional flows, but is relatively complex to implement in three dimensions[4,5]; and the other based on a direct numerical solution to the inviscid flow equations in noncharacteristic form. The latter approach relies on the technique of forward integration in a coordinate direction along which the local velocity component is everywhere supersonic. This method has been used by Babenko et al.[6]; and by Moretti, Abbett and Fort.[7] The latter work is restricted to perfect gas flow over an axisymmetric body.

In the present work, we develop a technique that is based on a similar procedure, but that is valid for real gas flow over smooth bodies of arbitrary shape. The validity of the technique is established by a comparison of numerical results with experimental data for blunt cones at incidence. Finally, a variety of results are presented for the more complicated case of a blunt delta wing at incidence.

Presented as Paper 71-596 at the AIAA 4th Fluid and Plasma Dynamics Conference, Palo Alto, Calif., June 21–23, 1971; submitted September 10, 1971; revision received January 31, 1972. This research was supported under the Lockheed Independent Research Program. The authors are indebted to H. Kirch, who was largely responsible for implementing the numerical method into an operational computer program.

Index category: Supersonic and Hypersonic Flow.

* Staff Scientist, Fluid Mechanics Laboratory.

† Staff Scientist, Fluid Mechanics Laboratory; now Lecturer in Mechanical Engineering, University of Santa Clara, Santa Clara, Calif.

‡ Research Scientist, Fluid Mechanics Laboratory.

2. Equations and Boundary Conditions

Equations

Consider the steady, compressible flow over a smooth convex body immersed in a uniform supersonic freestream. The equations governing the flow are

Continuity $$\nabla \cdot \rho \vec{V} = 0 \tag{1a}$$

Momentum $$\rho(\vec{V} \cdot \nabla)\vec{V} + \nabla p = 0 \tag{1b}$$

Constancy of entropy along streamlines

$$\vec{V} \cdot (\nabla p - c^2 \nabla \rho) = 0 \tag{1c}$$

where the sound speed is given as an arbitrary function $c = c(p, \rho)$.

These equations and all those that follow are written in dimensionless form: density is normalized by the freestream density ρ_∞, all speeds by the freestream speed V_∞, and pressure by the reference pressure $\rho_\infty V_\infty^2$. Distances are referenced to some characteristic body dimension.

Let the cylindrical coordinate system (r, ϕ, z) with associated velocity components (u, v, w) be fixed relative to the body, and oriented so that w is locally supersonic $(w > c)$ in the half-space $z \geqq z_0$. The Cauchy initial value problem is then well posed in terms of initial data given on the plane surface $z = z_0$. The solution is sought in that subregion R of the half-space bounded by the body surface $r = b(\phi, z)$ and an outer bow shock surface $r = s(\phi, z)$.

Under the conditions stated, Eqs. (1) may be solved explicitly for the z derivatives of the flow variables. When written in matrix notation, the system of equations takes the form

$$\vec{f}_z + A\vec{f}_r + B\vec{f}_\phi + \vec{g} = 0 \tag{2}$$

where the transpose of $\vec{f}$ is the row vector

$$(\vec{f})^T = (p, \rho, u, v, w) \tag{3}$$

that of $\vec{g}$ is

$$(\vec{g})^T = (1/r)(\rho c^2 uw/\eta, \rho uw/\eta, -v^2/w, uv/w, -c^2 u/\eta) \tag{4}$$

where

$$\eta = w^2 - c^2$$

and the coefficient matrices are

$$A = \eta^{-1}\begin{bmatrix} uw & 0 & \rho c^2 w & 0 & -\rho c^2 u \\ u/w & \eta u/w & \rho w & 0 & -\rho u \\ \eta/\rho w & 0 & \eta u/w & 0 & 0 \\ 0 & 0 & 0 & \eta u/w & 0 \\ -u/\rho & 0 & -c^2 & 0 & uw \end{bmatrix} \tag{5}$$

$$B = (r\eta)^{-1}\begin{bmatrix} vw & 0 & 0 & \rho c^2 w & -\rho c^2 v \\ v/w & \eta v/w & 0 & \rho w & -\rho v \\ 0 & 0 & \eta v/w & 0 & 0 \\ \eta/\rho w & 0 & 0 & \eta v/w & 0 \\ -v/\rho & 0 & 0 & -c^2 & vw \end{bmatrix} \tag{6}$$

The boundary condition at the body surface is

$$V_n = \vec{V}\cdot\vec{n} = 0 \tag{7}$$

where $\vec{n}$ is the outward unit vector normal to the surface.

The shock is a free boundary surface at which the Rankine-Hugoniot jump conditions apply as boundary conditions.

Equation (2) is to be solved numerically by forward integration in the z direction, subject to the described boundary conditions. The implementation of the numerical solution is greatly simplified if carried out in terms of a nonorthogonal coordinate system in which both body and shock are coordinate surfaces, rather than in terms of the original cylindrical coordinate system. This device has been utilized by Babenko et al.,[6] Moretti et al.,[1,7] Bastianon,[2] and others in solving flow problems of a similar nature. In terms of the new coordinates, computational mesh points are automatically constrained to lie along the shock and body boundary surfaces. This avoids tedious procedures of shock-fitting between mesh points, or of spatial interpolation to determine the flow variables at points of the body surface.

We shall restrict our attention to flows that have at least one plate of symmetry, which is taken to coincide with the meridional plane $\phi = 0$. Let ϕ_m, $0 < \phi_m \leqq \pi$ denote the upper limit of the angular region within which the flow is to be calculated. Normally, this will be the plane of symmetry $\phi_m = \pi$; however, the initial value problem remains well posed for $\phi_m < \pi$ as long as $v/c > 1$ everywhere in the plane $\phi = \phi_m$. We introduce a transformation from the physical coordinates to the nonorthogonal coordinates (X, Y, Z),

$$X = F[(r-b)/(s-b)], \quad Y = G(\phi/\phi_m, z), \quad Z = z \tag{8}$$

where the functions F and G must satisfy the monotonicity conditions $F_r > 0$, $G_\phi > 0$, but may otherwise be tailored to the requirements of a given problem. For convenience, we impose the conditions $F(0) = G(0,z) = 0$, $F(1) = G(1,z) = 1$, so that the transformation (8) maps the body and shock onto the surfaces $X = 0$ and $X = 1$, respectively. The flow region R is mapped into the semi-infinite rectangular solid $0 < X < 1, 0 < Y < 1, Z > Z_0$. Transformed to the new coordinates, Eq. (2) takes the form

$$\vec{f}_Z + C\vec{f}_X + D\vec{f}_Y + \vec{g} = 0 \tag{9}$$

with the new coefficient matrices

$$C = AF_r + BF_\phi + IF_z \tag{10}$$

$$D = BG_\phi + IG_z \tag{11}$$

where I is the identity matrix.

Boundary Conditions

Equation (9) is valid only in the interior of the flow region R. The flow at shock and body boundary surfaces is treated by the method described in Ref. 8. The method is based on the construction of specialized systems of differential equations that contain both the boundary conditions and the appropriate limiting form of the vector flow Eq. (9) at the boundary surface.

In spirit, the method is similar to that of Kentzer.[9] He obtained specialized systems of differential equations that govern the flow at the boundary surfaces by combining selected relations from the theory of characteristics with interior derivatives of the boundary conditions, but worked out the details only for two-dimensional flow. The present approach is outlined below for the three-dimensional case.

Body

At the body surface $X = 0$, Eq. (9) is valid in the limit as $X \to 0$ provided that the X derivatives are interpreted in the one-sided sense. However, the components of this vector equation are not linearly independent, but must satisfy the velocity boundary condition Eq. (7). A linearly independent subset may be found by analyzing the overdetermined system of equations comprised of the limiting form ($X \to 0$) of Eq. (9) and the Z derivative of the boundary condition.[8] However, the same results follow from the heuristic derivation given below.

We resolve the surface velocity vector into its components along two independent unit vectors $\vec{t}_1$ and $\vec{t}_2$ that lie in the local tangent plane

$$\vec{V} = V_1\vec{t}_1 + V_2\vec{t}_2 \tag{12}$$

It is convenient to choose the unit vectors as

$$\vec{t}_1 = \vec{n}\times\vec{e}_2/|\vec{n}\times\vec{e}_2|; \quad t_2 = \vec{t}_1\times\vec{n}/|\vec{t}_1\times\vec{n}|$$

where $\vec{e}_i$, $i = 1,2,3$ represent basic unit vectors in the (r, ϕ, z) coordinate directions, respectively. Upon inserting the expressions for $\vec{t}_1$ and $\vec{t}_2$ into Eq. (12) and differentiating the resulting equation with respect to Z holding X, Y constant (note that this represents an interior differentiation along the body surface $X = 0$), we find

$$V_{1Z} = \xi^{-1/2}(b_z u_Z + w_Z - \varepsilon v b_\phi/b\xi)$$

$$V_{2Z} = (\kappa\xi)^{-1/2}[b_\phi(u_Z - b_z w_Z)/b + \xi v_Z - \varepsilon(w + ub_z)b_\phi/b\xi]$$

where $\xi = 1 + b_z^2$, $\kappa = \xi + (b_\phi/b)^2$, and $\varepsilon = b_{zz} - b_{\phi z}G_z/G_\phi$. We then eliminate u_Z, v_Z, w_Z from these last equations by substituting the last three components of the limiting form of Eq. (9). There result two independent differential equations for V_{1Z} and V_{2Z}. We have not written down these equations explicitly because the algebra is tedious and unnecessary; the aforementioned substitution is most easily performed within the computer program that effects the numerical solution. Formally, however, these equations and the first two components of the limiting form ($X \to 0$) of Eq. (9) form a complete system of partial differential equations that governs the flow at the body surface.

Shock

A system that governs the flow at the shock surface is obtained in similar fashion. Under the assumption stated earlier that $\phi = 0$ represents a plane of symmetry, this plane must contain the freestream velocity vector $\vec{V}_\infty$. Then, if α denotes the angle of attack, and if the meridional angle ϕ is measured from the plane of symmetry on the windward side of the body, the components of $\vec{V}_\infty$ are

$$u_\infty = -\sin\alpha\cos\phi; \quad v_\infty = \sin\alpha\sin\phi; \quad w_\infty = \cos\alpha \tag{13}$$

The equations of conservation of mass, momentum, energy, and tangential velocity across the shock are well known, and need not be repeated here. If the energy conservation equation is written in terms of effective specific heat ratios γ_∞ and γ before and behind the shock, respectively, where γ is defined in terms of the dimensional pressure, density, and specific enthalpy by the equation

$$\gamma = [1 - p/\rho h)]^{-1} \tag{14}$$

then the shock relations may be solved explicitly in terms of the parameters γ, and shock pressure p. There result the following

expressions for the shock slope s_z, and for the density and velocity components behind the shock

$$(w_\infty{}^2 - U_\infty{}^2)s_z = w_\infty(u_\infty - v_\infty s_\phi/s) + U_\infty\{(w_\infty{}^2 - U_\infty{}^2)[1+(s_\phi/s)^2] + (u_\infty - v_\infty s_\phi/s)^2\}^{1/2} \quad (15)$$

$$\rho = \frac{\gamma+1}{\gamma-1}\left[\bar{p} + \frac{\gamma-1}{\gamma+1}\right]\left[\bar{p} + \frac{\gamma+1}{\gamma-1} + \frac{2(\gamma-\gamma_\infty)}{(\gamma-1)(\gamma_\infty-1)}\right]^{-1} \quad (16)$$

$$u = u_\infty + a \quad (17)$$

$$v = v_\infty - a(s_\phi/s) \quad (18)$$

$$w = w_\infty - as_z \quad (19)$$

where

$$\bar{p} = p/p_\infty \quad (20)$$

$$U_\infty{}^2 = [(\gamma+1)/2]p_\infty[\bar{p} + (\gamma-1)/(\gamma+1)] \times [1 + (\gamma_\infty - \gamma)/(\gamma_\infty - 1)(\bar{p}-1)]^{-1} \quad (21)$$

$$a = \frac{2}{\gamma+1}\left[\frac{-u_\infty + v_\infty(s_\phi/s) + w_\infty s_z}{1 + s_z{}^2 + (s_\phi/s)^2}\right]\left[\frac{\bar{p} - (\gamma-1)/(\gamma_\infty-1)}{\bar{p} + (\gamma-1)/(\gamma+1)}\right] \quad (22)$$

If Eqs. (14–19) are supplemented by the equation of state $h = h(p, \rho)$, there results a set of seven relations among the eight unknowns p, ρ, h, γ, u, v, w, and s_z. The variable s_ϕ is regarded as known, since it may be computed in terms of s from a difference formula.

It can be shown that any one of the components of the limiting form of Eq. (9) as $X \to 1$ constitutes an eighth independent relation with which to close the system of shock equations. For computational accuracy, it is preferable to use the first component of Eq. (9), viz., the differential equation for the pressure. One then has a complete system of equations that governs the flow at the shock.

The validity of the foregoing procedure follows from an analysis of the overdetermined linear system comprised of Eq. (9) and the Z derivatives of Eqs. (15–19) (interior derivatives along the shock surface). The proof is lengthy and will be presented elsewhere.[8] Finally, we note that use of the parameter γ defined by Eq. (14) involves no approximation, but is valid in general for any gas in local thermodynamic equilibrium. For either perfect gas flow ($\gamma = \gamma_\infty$) or for frozen flow behind the shock ($\gamma \neq \gamma_\infty$), γ is a constant and the shock solution is explicit. In other cases, γ varies with the thermodynamic state, but is a convenient iteration parameter for obtaining a convergent iterative solution to the shock relations.

3. Difference Equations

The equations developed previously are solved by forward integration in the Z direction. To effect the numerical solution, the domain of integration is subdivided into a uniform rectangular mesh, with intervals $\Delta X = 1/N$, $\Delta Y = 1/M$. The integers N, M may be unequal. The coordinates of the computational mesh points (X_i, Y_j) are

$$X_i = (i-1)\Delta X, \quad i = 1, 2, \ldots, N+1$$
$$Y_j = (j-2)\Delta Y, \quad j = 1, 2, \ldots, M+3 \quad (23)$$

where the extra rows of mesh points $j = 1$ and $j = M+3$ are included to facilitate the application of boundary conditions at $Y = 0$ and $Y = 1$.

At interior points, the following modified form of MacCormack's predictor-corrector scheme[10] is used to advance the solution of Eq. (9) by one integration step from the plane $Z = Z^n$ to the plane Z^{n+1}:

Predictor

$$\tilde{\vec{f}}_{ij}{}^{n+1} = \vec{f}_{ij}{}^n - (\Delta Z/\Delta X)C_{ij}{}^n(\vec{f}_{i+1,j}{}^n - \vec{f}_{ij}{}^n) - (\Delta Z/\Delta Y)D_{ij}{}^n(\vec{f}_{i,j+1}{}^n - \vec{f}_{ij}{}^n) - \Delta Z\vec{g}_{ij}{}^n \quad (24a)$$

Corrector

$$\vec{f}_{ij}{}^{n+1} = \tfrac{1}{2}\{\vec{f}_{ij}{}^n + \tilde{\vec{f}}_{ij}{}^{n+1} - (\Delta Z/\Delta X)\tilde{C}_{ij}{}^{n+1}(\tilde{\vec{f}}_{ij}{}^{n+1} - \tilde{\vec{f}}_{i-1,j}{}^{n+1}) - (\Delta Z/\Delta Y)\tilde{D}_{ij}{}^{n+1}(\tilde{\vec{f}}_{ij}{}^{n+1} - \tilde{\vec{f}}_{i,j-1}{}^{n+1}) - \Delta Z\tilde{\vec{g}}_{ij}{}^{n+1}\} \quad (24b)$$

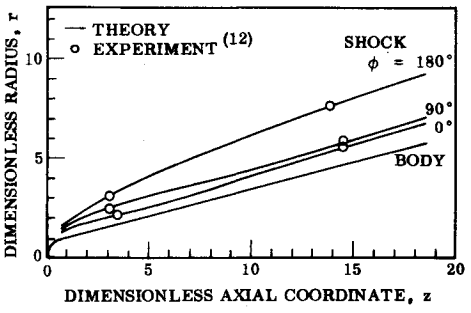

Fig. 1 Shock shape over a blunt 15° cone, $\gamma = 1.4$, $V_\infty/c_\infty = 10.6$, $\alpha = 10°$.

The scheme is of uniform second-order accuracy. MacCormack[10] has shown that, for the one-dimensional unsteady flow equations in conservation law form, the stability of the scheme is governed by the well-known Courant-Friedrichs-Lewy (CFL) condition. It is easy to establish the corresponding result for the two-dimensional steady supersonic flow equations in the common Euler form that is used in the present work [Eq. (9)]. Apparently, no rigorous stability limit has yet been established for the scheme when applied to multi-dimensional flow, steady or unsteady. Nevertheless, the three-dimensional steady flow computations that will be described later were performed successfully with a stepsize ΔZ chosen as a substantial fraction (usually 0.9) of the minimum value given by local application of the CFL condition at all mesh points.

The boundary conditions are treated numerically in the following manner: At the plane of symmetry, $Y = 0$, the exact boundary conditions are

$$v = p_\phi = \rho_\phi = u_\phi = w_\phi = s_\phi = b_\phi = 0$$

These are satisfied in the usual manner according to the reflection principle by assigning appropriate values to the flow variables $\vec{f}_{ij}$ at the fictitious mesh point $j = 1$:

$$v_{ij} = \{1 - 2\Delta Y/\phi_{i,j+2}[G_\phi(0, z)]\}v_{i,j+2}$$
$$p_{ij} = p_{i,j+2}, \rho_{ij} = \rho_{i,j+2}, \text{ etc.}$$

When $\phi_m = \pi$, similar conditions are applied at $j = M+3$; for $\phi_m < \pi$, the values of the flow variables are extrapolated from interior points.

To maintain second-order accuracy, it is necessary to first complete the predictor for all mesh points, including those at shock and body boundaries, before applying the corrector. The flow variables at those boundary points are computed by apply-

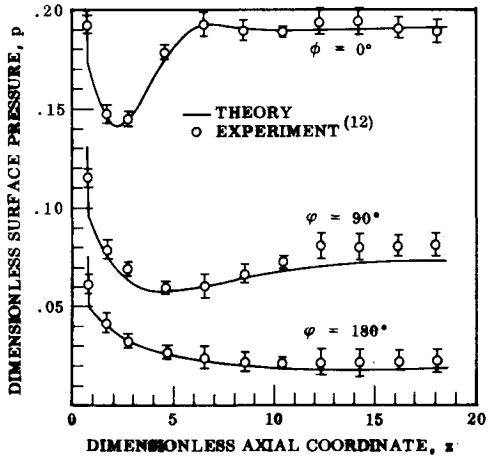

Fig. 2 Axial surface pressure distribution on a blunt 15° cone, $\gamma = 1.4$, $V_\infty/c_\infty = 10.6$, $\alpha = 10°$.

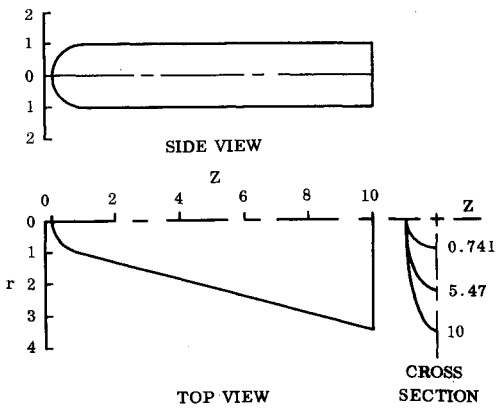

Fig. 3 Delta body geometry.

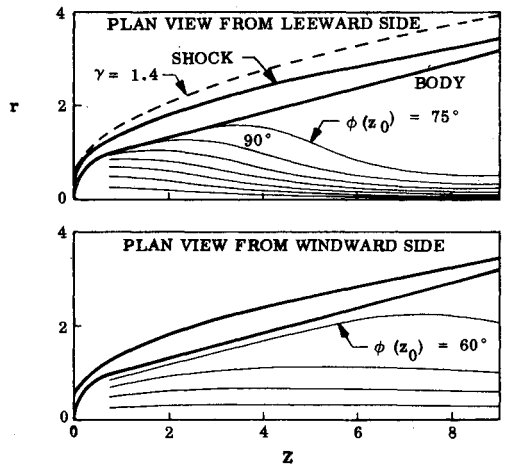

Fig. 5 Plan views of shock shape and surface streamline pattern, delta body, $\alpha = 10°$.

ing Eq. (24) to the specialized systems of differential equations developed earlier, except that purely one-sided difference formulas are used in evaluating $\bar{f}_X$. That is, the differences are taken in the same direction in both predictor and corrector.

In the shock computations, s_ϕ is evaluated from a central difference formula. Once Eq. (15) and the first component of Eq. (9) are integrated, the remaining variables are computed from the algebraic shock relations. For a general equilibrium gas, this involves an iteration on the value of the parameter γ, as noted earlier.

4. Numerical Results

Selected results of computations of three-dimensional flow over spherically blunted bodies are presented in Figs. 1–18. The notation is as follows. The body shape is specified in cylindrical coordinates (r, ϕ, z), with r and z referred to the nose radius and ϕ (the meridional angle) measured from the windward plane of symmetry. The dimensionless radial coordinates of the shock and body are s and b, respectively. The angle of attack is denoted by α. The dimensionless pressure p is referred to $\rho_\infty V_\infty^2$, the dimensionless enthalpy h to $V_\infty^2/2$, and the dimensionless density ρ to ρ_∞.

Validation of Solution Technique

The described techniques have been tested on a number of problems having known solutions. For sharp cones at various angles of attack, very close agreement has been obtained with results published by Babenko.[6] Calculations have also been performed for spherically blunted cones at incidence, using initial data obtained from the computer programs developed by Inouye, Rakich, and Lomax[11] for the subsonic and transonic parts of the flow. The results agree well with experimental data[12] and with existing method of characteristics solutions.[5]

A typical comparison with experimental data on surface pressure distribution and shock shape is displayed in Figs. 1 and 2. The theoretical results were computed using simple linear functions in the coordinte transformation, Eq. (8)

$$F = (r-b)/(s-b) \qquad G = \phi/\phi_m, \phi_m = \pi \tag{25}$$

The error bars on the experimental data of Fig. 2 do not appear in the original reference.[12] They were calculated for present purposes from the scatter among the data points for various meridional planes in axisymmetric flow ($\alpha = 0$).

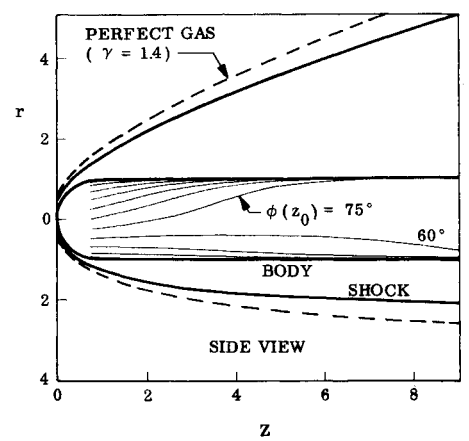

Fig. 4 Side view of shock shape and surface streamline pattern, delta body, $\alpha = 10°$.

Solutions for a Delta Body

The numerical technique has also been used to compute the flow about the spherically blunted 75° swept delta body illustrated in Fig. 3. The body is bilaterally symmetric with straight leading edges and an elliptical cross section, and is continuously tangent to the spherical nose.

The body shape aft of $z = z_0$, the plane of juncture with the spherical nose, is given by

$$b = [A^{-2}\sin^2\phi + B^{-2}\cos^2\phi]^{-1/2}, \quad z \geq z_0 \tag{26}$$

The major and minor semiaxes of the elliptical cross section are, respectively,

$$A = \cos\theta + (z-z_0)\tan\theta \tag{27a}$$

$$B = (\cos\theta)^{1/m} \tag{27b}$$

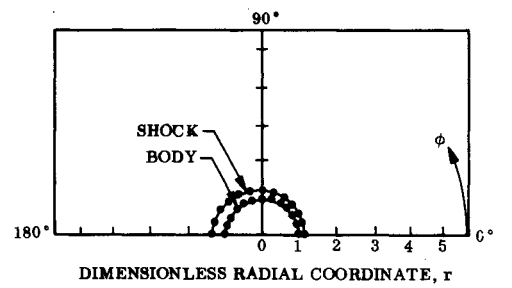

Fig. 6 Polar plot of delta body and shock shapes at initial data plane $z = z_0 = 0.741$, $\alpha = 10°$.

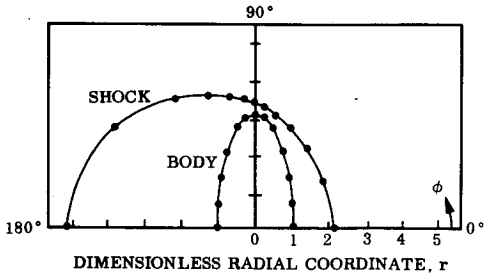

Fig. 7 Polar plot of delta body and shock shapes at $z = 9$, $\alpha = 10°$.

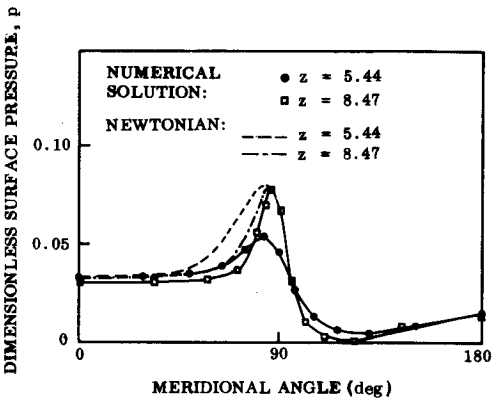

Fig. 9 Comparison of Newtonian approximation with numerical solution, delta body, $\alpha = 10°$.

where θ denotes the complement of the leading-edge sweepback angle, and

$$m = 1-(z-z_0)\sin\theta/(\cos^2\theta)\ln(\cos\theta)$$

The minor semiaxis exponentially approaches a constant value equal to the nose radius of curvature so that the root thickness is very nearly constant for $z > 1$.

The following nonlinear coordinate transformation functions were used in the flow computations:

$$F = (1/\omega)\sinh^{-1}[\{(r-b)/(s-b)\}\sinh\omega] \quad (28a)$$

$$G = Y_0+(1/\beta)\sinh^{-1}[(\phi/\phi_0-1)\sinh\beta Y_0] \quad (28b)$$

where ϕ_0 is a given meridional angle, and

$$Y_0 = \frac{1}{2\beta}\ln\left[\frac{1+(e^{\beta}-1)\phi_0/\phi_m}{1-(1-e^{-\beta})\phi_0/\phi_m}\right]$$

is its image in the transformed space. The inverse hyperbolic functions represent a nonlinear stretching of the physical coordinates that is employed to improve the spatial resolution of the numerical solution in regions of steep gradients. For example, far downstream of the nose, the high-entropy gas that passed through a nearly normal bow shock is confined to a thin layer near the body surface. Within this entropy layer, large radial gradients exist in the flow variables. The stretching function allows one to focus the computational mesh points within the layer, with the density of points in physical space controlled by the magnitude of the coefficient ω. The spatial resolution and computational accuracy are improved in the region of steep gradients without an increase in the total number of mesh points, and without our being forced to abandon the operationally convenient uniform mesh spacing ΔX, ΔY in the computational space. We note that the allowable integration step size is adversely affected because it is related through the CFL condition to the mesh spacing in the z = const plane. This penalty exists for any conditionally stable differencing scheme. However, most such schemes are sensitive to the degree of spatial resolution in a way that is not entirely accounted for by the linear stability analysis that leads to the CFL criterion. We have found that inadequate resolution can cause disastrous instabilities regardless of the step size. The coordinate stretching technique is clearly the most efficient way to obtain adequate resolution in such cases.

The angular coordinate transformation, Eq. (28b), has a similar purpose; mesh points are concentrated near the plane $\phi = \phi_0$. For the delta body, the greatest angular variation in flow variables occurs near the leading edge, and we choose $\phi_0 = \pi/2$.

Numerical results for the entire flowfield ($\phi_m = \pi$) at low angles of attack are displayed in Figs. 4–14. All computed results for the described delta body are for air in chemical equilibrium at the typical space shuttle orbiter freestream conditions of 20,000 fps at 200,000 ft altitude. Figure 4 shows shock and body shapes in the plane of symmetry of the flowfield for an angle of attack $\alpha = 10°$. Also shown are selected surface streamlines projected onto the plane of symmetry. The streamlines shown are those that pass through the initial data plane $z = z_0 = 0.7412$ at meridional locations $\phi(z_0)$ equally spaced at 15° intervals. For comparison, the shock shape for perfect gas flow is also given (dashed curve). A similar plot for the $\phi = 90°$ plane of symmetry of the body is given in Fig. 5. A striking feature is the tendency of the shock to converge toward the leading edge of the wing far downstream of the nose. This phenomenon has been observed in experimental studies of the flowfield over flat, blunted delta wings.[13] The increasing asymmetry of the flowfield with distance

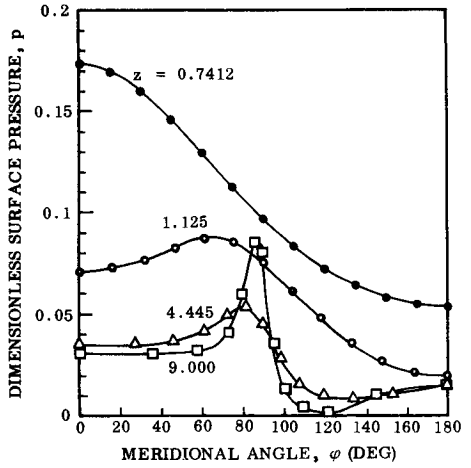

Fig. 8 Meridional surface pressure distributions, delta body, $\alpha = 10°$.

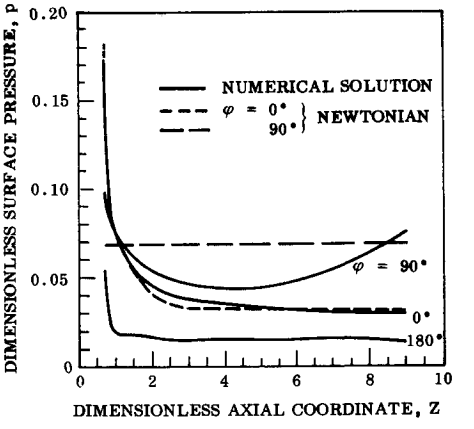

Fig. 10 Axial surface pressure distributions, delta body, $\alpha = 10°$.

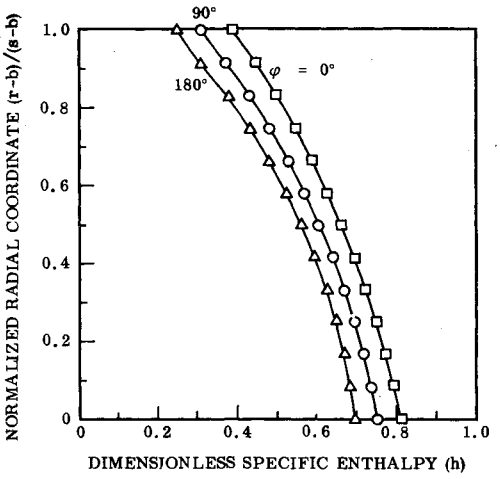

Fig. 11 Radial profiles of specific enthalpy at $z = z_0$, delta body, $\alpha = 10°$.

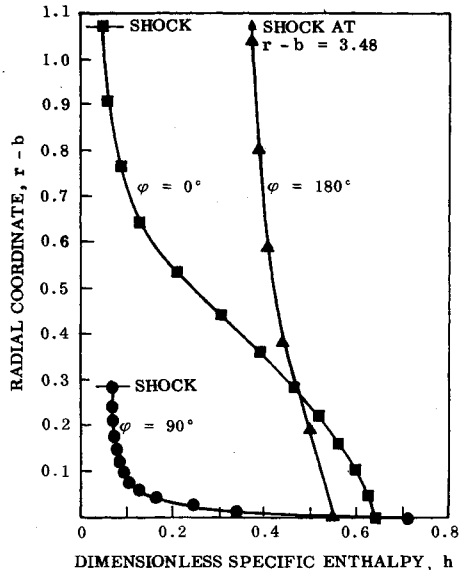

Fig. 13 Radial profiles of specific enthalpy at $z = 8.47$, plotted in physical coordinates; delta body, $\alpha = 10°$.

from the nose is illustrated by the polar plots of shock and body shape presented in Figs. 6 and 7.

The surface streamline patterns of Figs. 4 and 5 suggest the existence of a "shedding" streamline that originates at a meridional angle $\phi(z_0)$ slightly in excess of 60°, and remains on the windward surface. Streamlines originating at larger meridional angles are quickly swept onto the leeward surface of the body, whereas streamlines originating at lower angles $\phi(z_0) < 60°$ remain on the windward surface. The windward surface streamlines initially tend to approach the leading edge, but, farther downstream, reverse their direction and tend to converge toward the windward plane of symmetry.

This behavior is consistent with the nature of the surface pressure distributions plotted in Fig. 8. The meridional pressure distribution is initially monotonic at $z = z_0$; however, within a short distance downstream, there develops the sharp leading-edge peak characteristic of a wing, and streamlines are driven away from the point of peak pressure.

Also evident in Fig. 8 is a recompression region near the leeward plane of symmetry for $z \gtrsim 4$. For example, at $z = 9$, the cross flow is subsonic ($v/c < 1$) everywhere on the windward surface. As it passes over the leading edge onto the leeward side of the body, the flow undergoes a violent expansion up to $\phi \approx 120°$ at which point the cross flow is supersonic. The expansion is followed by a strong recompression (a tenfold increase in pressure) between $\phi = 120°$ and 145° that suggests the existence of a lee-side shock. The MacCormack differencing scheme involves an implicit dissipation of fourth order, and has been used successfully with the conservation-law form of the flow equations to compute shock transitions.[10,14] The present results indicate that, in the case of weak shocks, such computations are also possible with the Euler form of the equations, although a finer mesh spacing $\Delta\phi$ would be required to resolve the shock adequately in the present case. The restriction to weak shocks is a consequence of our employing Eq. (1c), which disallows any change in entropy along streamlines. This approximation is good across a weak shock but deteriorates rapidly with increasing shock strength.

The simple Newtonian approximation§

$$p = p_\infty + (\vec{V}_\infty \cdot \vec{n})^2 \tag{29}$$

is sometimes used to estimate the windward surface pressure distribution for preliminary design purposes; it is of some interest, therefore, to compare the approximation with the present numerical solution. Figure 9 shows such a comparison for the meridional pressure distribution at several axial locations.

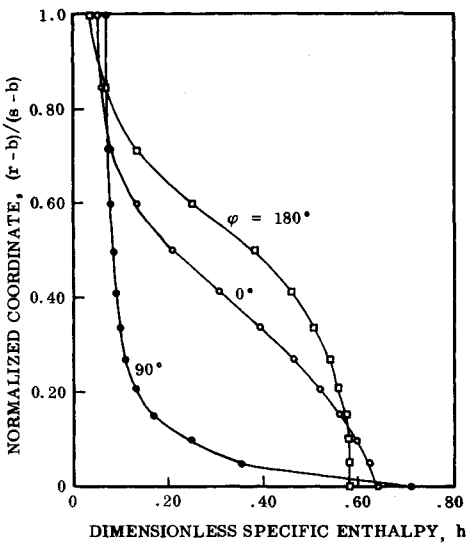

Fig. 12 Radial profiles of specific enthalpy at $z = 8.47$, delta body, $\alpha = 10°$.

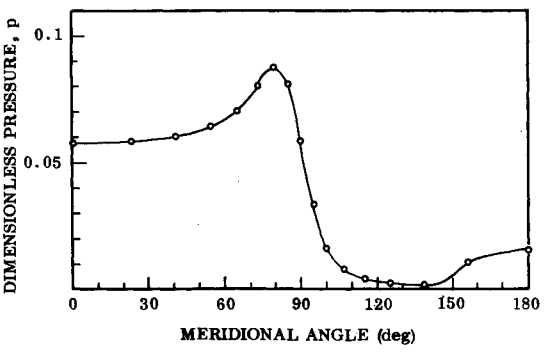

Fig. 14 Meridional surface pressure distribution at $z = 5.7$, delta body, $\alpha = 15°$.

§ The reader is reminded that all pressures are normalized by the freestream momentum flux $\rho_\infty V_\infty^2$.

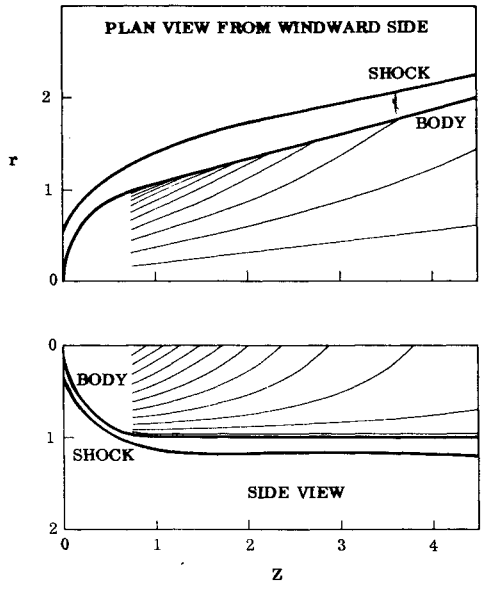

Fig. 15 Plan and side views of shock shape and windward surface streamline patterns, delta body, $\alpha = 30°$.

At this low angle of attack, the Newtonian approximation is rather poor except in the neighborhood of the plane of symmetry ($\phi = 0$). The approximation improves with increasing distance from the nose, and differs by less than 20% from the numerical solution at $z = 9$. Axial surface pressure distributions in selected meridional planes are shown in Fig. 10.

An important aspect of the flow is the structure of the entropy layer, because of its influence on surface heat transfer. Near the nose, the radial distributions of static enthalpy are similar in character at various meridional locations, as shown in Fig. 11. Far downstream, however, the behavior is much different. Figure 12 shows the computed enthalpy distributions at $z = 8.47$ for the same meridional planes as in Fig. 11. Because of the large cross flow in the vicinity of the leading edge, the entropy layer thickness is reduced to a small fraction of the local shock layer thickness. The entropy layer thickness remains of the same order as the shock layer thickness near both windward and leeward planes of symmetry, where cross flow effects are less pronounced.

The enthalpy profiles are replotted in Fig. 13 in physical coordinates to display the relative steepness of the enthalpy gradient at the wall near the leading edge. These results indicate

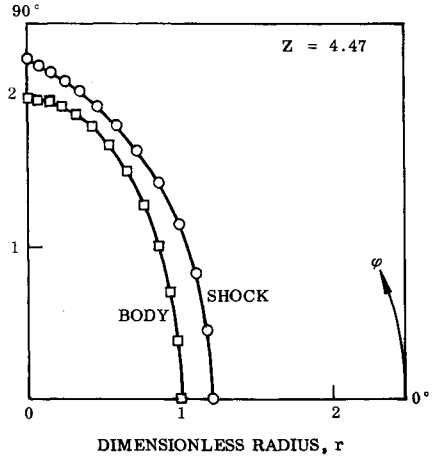

Fig. 16 Polar plot of delta body and shock shape at $z = 4.47$ for $\alpha = 30°$.

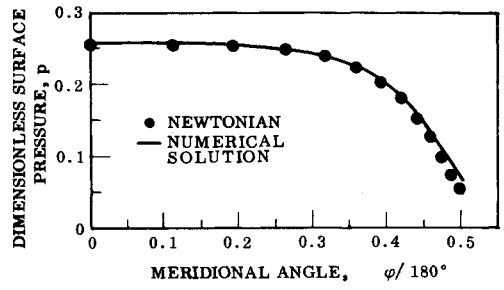

Fig. 17 Meridional surface pressure distribution at $z = 4.47$, delta body, $\alpha = 30°$.

that, at low angles of attack, the effects of external vorticity on boundary-layer heat-transfer predictions are likely to be much more important near the leading edge than elsewhere on the body surface.

As the angle of attack is increased, the windward-surface pressure peak near the leading edge becomes less pronounced, primarily because the pressure is increased over the remainder of the windward surface. This is illustrated by comparison of the meridional surface pressure distribution of Fig. 14 ($\alpha = 15°$) with that of Fig. 8. The over-all structure of the flowfield remains qualitatively similar in character to that for $\alpha = 10°$. Quantitatively, however, the entropy layer thickness over the windward surface as a whole at a given axial position tends to be reduced with increasing angle of attack because of the larger cross flow.

At sufficiently high angles of attack, the leading-edge pressure peak disappears completely, and the entropy layer tends to become more uniform in structure over the entire windward surface. Numerical results for the flow over the windward surface ($\phi_m = \pi/2$) at 30° angle of attack are given in Figs. 15–18. Figure 15 shows the shock shape and surface streamline pattern for streamlines $\phi(z_0)$ at intervals of approximately 8°. The shock layer is significantly thinner than at low angles of attack, and shows less tendency to approach the leading edge. The surface streamlines diverge unabated from the windward plane of symmetry.

The polar plot of Fig. 16 shows that, except for a small region near the leading edge, the shock shape is more nearly concentric with the body than at low angle of attack. Under these conditions, the Newtonian approximation would be expected to be reasonably good. This expectation is borne out by the meridional surface pressure distribution given in Fig. 17; the Newtonian values agree with the numerical solution to within a few per cent everywhere outside a small region near the leading edge. Note the absence of the leading-edge pressure peak that appears in the results for low angles of attack.

The entire windward surface is dominated by large cross flow effects, although the effects remain more severe near the leading

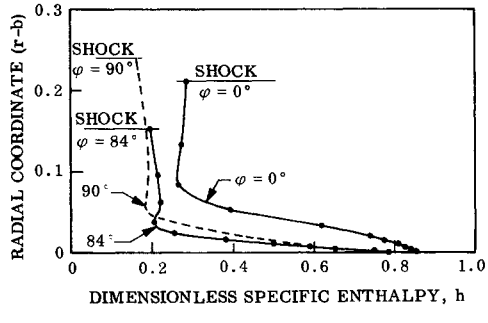

Fig. 18 Radial profiles of specific enthalpy at $z = 4.94$, delta body, $\alpha = 30°$.

edge (see Fig. 15). As a result, the entropy layer becomes thin much nearer the nose than at low angles of attack. The radial profiles of static enthalpy shown in Fig. 18 illustrate the steep gradients that occur at the wall over the entire windward surface. The results indicate that for the windward surface, the effects of external vorticity on boundary-layer heat-transfer predictions will become important much nearer the nose the larger the angle of attack.

5. References

[1] Moretti, G. and Bleich, G., "Three-Dimensional Flow Around Blunt Bodies," *AIAA Journal*, Vol. 5, No. 9, Sept. 1967, pp. 1557–1562.

[2] Bastianon, R., "Unsteady Solution of the Flow Field Over Concave Bodies," *AIAA Journal*, Vol. 7, No. 3, March, 1969, pp. 531–533.

[3] Barnwell, R. W., "Three-Dimensional Flow Around Blunt Bodies with Sharp Shoulders," AIAA Paper 71-56, New York, 1971.

[4] Chu, C. W., "Compatibility Relations and a Generalized Finite-Difference Approximation for Three-Dimensional Steady Supersonic Flow," *AIAA Journal*, Vol. 5, No. 3, March 1967, pp. 493–501.

[5] Rakich, J. V. and Cleary, J. W., "Theoretical and Experimental Study of Supersonic Flow Around Inclined Bodies of Revolution," *AIAA Journal*, Vol. 8, No. 3, March 1970, pp. 511–518.

[6] Babenko, K. I., Voskresenskiy, G. P., Lyubimov, A. N., and Rusanov, V. V., "Three-Dimensional Flow of an Ideal Gas Past Smooth Bodies," TT-F-380, April 1966, NASA.

[7] Moretti, G., Abbett, M. J., and Fort, R., "Three-Dimensional Inviscid Flow About Supersonic Blunt Cones at Angle of Attack," III: "Coupled Subsonic and Supersonic Programs," SC-CR-68-3728, Sept. 1968, Sandia Labs., Albuquerque, N. Mex.

[8] Thomas, P. D., "On the Computation of Boundary Conditions in Finite-Difference Solutions for Multidimensional Inviscid Flow Fields," LMSC 6-82-71-3, March 1971, Lockheed Palo Alto Research Lab., Palo Alto, Calif.; also *Journal of Computational Physics*, to be published.

[9] Kentzer, C. P., "Discretization of Boundary Conditions on Moving Discontinuities," *Proceedings of the Second International Conference on Numerical Methods in Fluid Dynamics, Lecture Notes in Physics*, Vol. 8, 1971, pp. 108–113.

[10] MacCormack, R. W., "The Effect of Viscosity in Hypervelocity Impact Cratering," AIAA Paper 69-354, Cincinatti, Ohio, 1969.

[11] Inouye, M., Rakich, J. V., and Lomax, H., "A Description of Numerical Methods and Computer Programs for Two-Dimensional and Axisymmetric Supersonic Flow over Blunt-Nosed and Flared Bodies," TN-D-2970, Aug. 1965, NASA.

[12] Cleary, J. W., "An Experimental and Theoretical Investigation of the Pressure Distributions and Flow Fields of Blunted Cones at Hypersonic Mach Numbers," TN-D-2969, Aug. 1965, NASA.

[13] Bertram, M. H. and Everhart, P. E., "An Experimental Study of the Pressure and Heat Transfer Distribution on a 70° Sweep Slab Delta Wing in Hypersonic Flow," TR-R-153, Dec. 1963, NASA.

[14] Kutler, P., "Application of Selected Finite-Difference Techniques to the Solution of Conical Flow Problems," Ph.D. thesis, Oct. 1969, Iowa State Univ., Ames, Iowa.